Chemical Science

ROYAL SOCIETY OF CHEMISTRY

EDGE ARTICLE

View Article Online
View Journal | View Issue

Cite this: *Chem. Sci.*, 2025, **16**, 9920

All publication charges for this article have been paid for by the Royal Society of Chemistry

Received 24th December 2024
Accepted 27th April 2025

DOI: 10.1039/d4sc08696a

rsc.li/chemical-science

Oxidation-induced double aromaticity in periodo-polycyclic hydrocarbons†

Slađana Đorđević, [a] Jordi Poater, [b] Miquel Solà *[cd] and Slavko Radenković *[a]

The doubly oxidized hexaiodobenzene $[C_6I_6]^{2+}$ is a well-known example of a double aromatic molecule, exhibiting both π- and σ-aromaticity. In this study, a series of periodo-monocyclic molecules and their doubly oxidized forms were systematically investigated to explore the origin of their double aromaticity. These molecules were employed to provide insights into how the size and aromaticity of the central carbon atom ring influence the aromaticity of the resulting doubly oxidized structures. The knowledge gained in this study was subsequently applied to model periodo-derivatives of polycyclic (anti)aromatic hydrocarbons in which oxidation can induce additional σ-electron cyclic delocalization along the macrocyclic iodine ring, thus also achieving their double aromaticity.

Introduction

Aromaticity has historically been associated with the cyclic delocalization of π-electrons. However, it later became clear that σ-electrons can also participate in a similar type of cyclic delocalization, giving rise to the concept of σ-aromaticity.[1–3] In 1979, Schleyer introduced the idea of double aromaticity, of both π and σ natures.[4] According to this author, the doubly aromatic molecule features two orthogonal cyclically delocalized electronic systems. The initial model proposed for the concept was the cationic $C_6H_3^+$,[4] which has been later experimentally characterized.[5] A significant advancement in the understanding of double aromaticity was made by Sagl and Martin who synthesized the $C_6I_6^{2+}$ dication.[6] Their comprehensive study demonstrated that $C_6I_6^{2+}$ is a stable system with a singlet ground state. Furthermore, they found that the geometric and magnetic properties of this molecule indicate the presence of both π- and σ-aromaticity. In more recent work, Saito *et al.* successfully synthesized and characterized hexakis(phenylselenyl)benzene dication.[7] This molecule features a π-aromatic benzene unit, together with σ-aromatic ring formed by selenium atoms.

Double aromaticity has been extensively studied, with $C_6I_6^{2+}$ often serving as a prototypical example of this phenomena.[8–10] This double aromaticity was substantiated by the calculation of ring current, NICS, aromatic stabilization energy, and electronic indices.[8–13] However, double aromaticity has also been identified in numerous molecules that do not necessarily contain a benzene core structure. Recent research by Escayola *et al.* examined double aromaticity in perhalogen-tropylium cation in both singlet and triplet states.[11] Among the systems studied, only triplet $C_7Br_7^{+3}$ with an internal Hückel aromatic tropylium ring (6 π-electrons) and an external incipient Baird aromatic Br_7^{+2} ring (12 σ-electrons) showed double π- and σ-aromaticity. Fowler and Havenith explored periodo-cyclooctatetraene derivatives, $C_8I_8^q$ with charges $q = 0$, +1, ±2, and +4.[14] However, the large I–I steric repulsion in these periodo-cyclooctatetraene species led to highly puckered structures with lack of both σ- and π-aromaticity. Additionally, double aromaticity has proven to be a valuable concept for explaining and rationalizing the structure and stability of various pure and doped boron clusters.[15–17] It has also been thoroughly investigated in C_n monocyclic clusters possessing π_{in} and π_{out} orthogonal (anti) aromaticities.[18–27] Moreover, double 3D-aromaticity has been analyzed in the $B_{12}I_{12}$ cluster,[12,13] but the authors found that, despite many favorable evidences, the potential double 3D-aromaticity of the I_{12} shell did not contribute to any stabilization of the system and, consequently, it was concluded that this cluster does not display double aromaticity.

As demonstrated experimentally by Sagl and Martin,[6] and confirmed in numerous computational studies,[8–10] oxidation of the neutral C_6I_6, which is π-aromatic, induces σ-aromaticity, resulting in the formation of the doubly aromatic dication $C_6I_6^{2+}$. This oxidation process removes two electrons from the HOMO, which is a σ-orbital, and consequently, this leads to the existence of two Hückel aromatic cyclic systems: π-system with 6 and σ-system with 10 electrons. In nearly all previous studies on the double aromaticity of periodo-derivatives, the core carbon structure exhibits a monocyclic structure. In this contribution, we aim

[a]*University of Kragujevac, Faculty of Science, P. O. Box 60, 34000 Kragujevac, Serbia. E-mail: slavkoradenkovic@kg.ac.rs*

[b]*Departament de Química Inorgànica i Orgànica & IQTCUB, Universitat de Barcelona, 08028 Barcelona, Spain*

[c]*ICREA, Pg. Lluís Companys 23, 08010 Barcelona, Spain*

[d]*Institut de Química Computacional i Catàlisi and Departament de Química, Universitat de Girona, 17003 Girona, Catalonia, Spain. E-mail: miquel.sola@udg.edu*

† Electronic supplementary information (ESI) available. See DOI: https://doi.org/10.1039/d4sc08696a

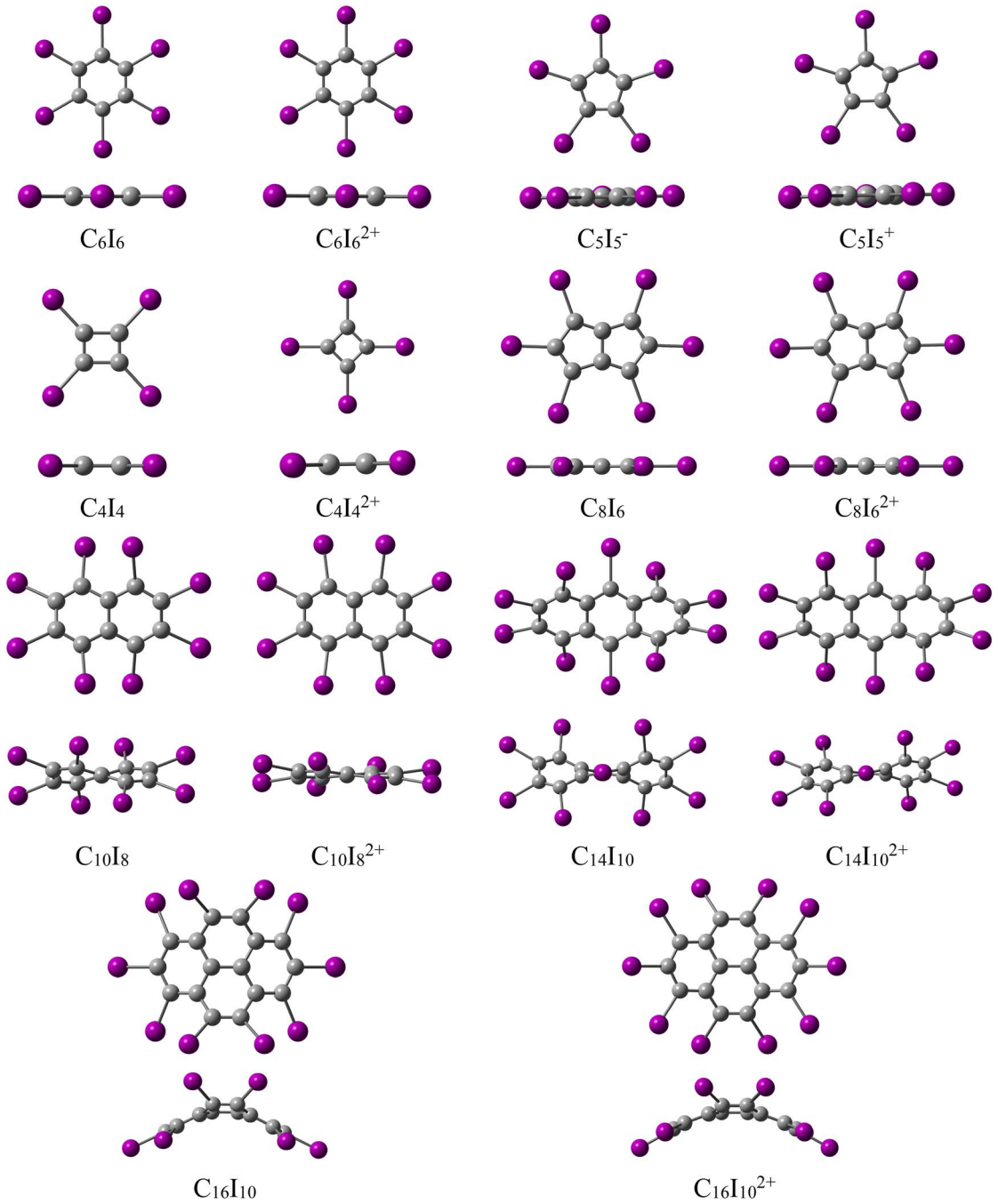

Fig. 1 Top and side views of optimized structures for the studied periodated molecules and their oxidized forms.

to address the following questions: can σ-aromaticity be induced by oxidizing a periodo-system that has a polycyclic core structure, where the iodine atoms form a macrocycle? We will start our investigation with a series of monocyclic periodo-derivatives (Fig. 1). These systems will help us understand how the size and aromatic character of the central ring influence the aromaticity of the resulting doubly oxidized system. In the second part of this study, we will examine a series of periodo-polycyclic hydrocarbons and their doubly oxidized forms (Fig. 1). To assess the extent of aromaticity in the studied molecules, we utilize two electronic indices (multicentre index (I_{ring})[28] and electron density of delocalized bonds (EDDB)[29,30]), along with a magnetic indicator, the magnetically induced current density (MICD)[31–33] and an energetic measure, namely the aromatic stabilization energy.[34,35]

Results and discussion

Periodo-monocyclic (anti)aromatic hydrocarbons

The double aromaticity of periodo-benzene dication has been demonstrated in numerous studies using various aromaticity descriptors.[8–11] The MICD map for periodo-benzene reveals its π-aromatic character, showing intensive diatropic circulations

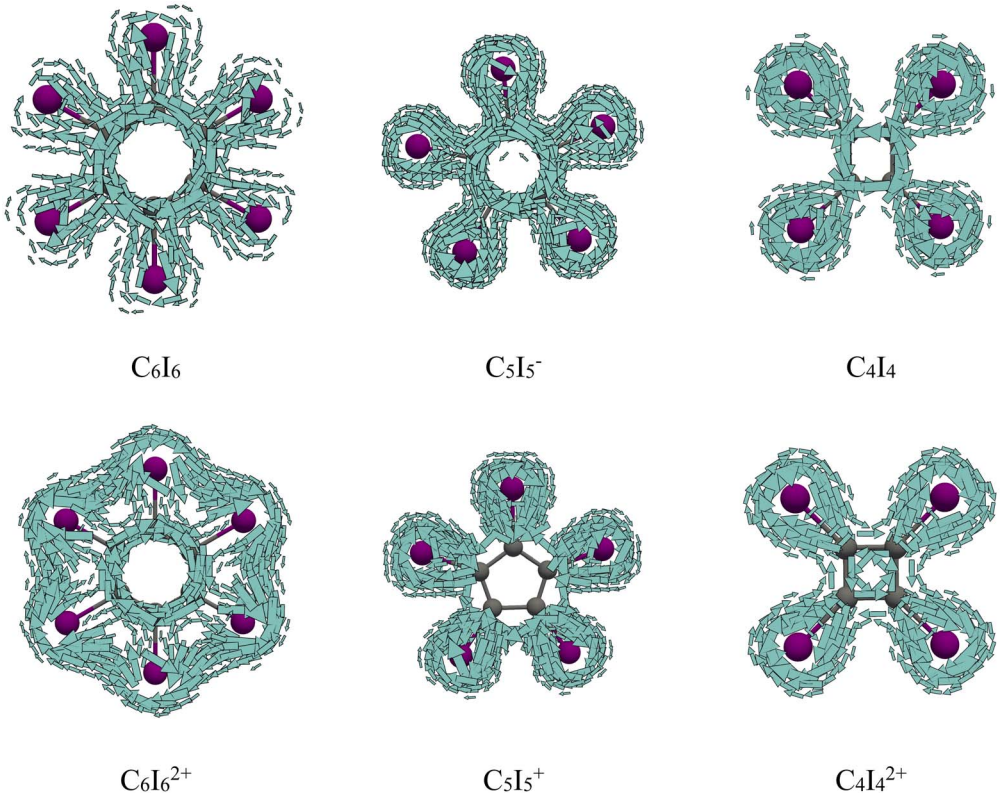

Fig. 2 Total current density maps plotted 1 Bohr above molecular plane for C_6I_6, $C_6I_6^{2+}$, $C_5I_5^-$, $C_5I_5^+$, C_4I_4, and $C_4I_4^{2+}$.

along the benzene ring and only local circulations around the iodine atoms (Fig. 2). On the other hand, the current density map of $C_6I_6^{2+}$ displays two distinct diatropic circulations: one along the benzene ring and another along the iodine atom ring. The current density in these molecules can be dissected into contributions of π- and σ-electrons (Fig. 3). In what follows, π-MOs are considered as those having the main contributions from p_z-atomic orbitals on carbon atoms (assuming that the carbon atoms lie in the *xy*-plane), while σ-MOs are those having the dominant contributions from the in-plane 5p atomic orbitals of iodine atoms (Fig. S1†). As shown in Fig. 3, the π-electrons induce diatropic currents in both C_6I_6 and $C_6I_6^{2+}$. Furthermore, in $C_6I_6^{2+}$, the σ-electrons induce diatropic currents, whereas in C_6I_6 there are only local circulations around the iodine atoms. The observed magnetic aromaticity can be understood within the framework of Hückel's 4n + 2 rule.[36] In C_6I_6, there are 6 and 12 electrons in the π- and σ-electron molecular subgroup, respectively (Fig. S1†). Since the σ-MO subgroup is fully occupied, it does not show any significant magnetic response. Upon oxidation, the number of σ-electrons is reduced to 10, while the number of π-electrons remains unchanged.

The double aromaticity of periodo-derivatives of cyclopentadienyl anion and cyclobutadiene, as well as their doubly oxidized forms, is examined below. In $C_5I_5^-$, diatropic currents are observed within the five-membered ring, similar to those in cyclopentadienyl anion itself, while no global circulations occur along the perimeter formed by the iodine atoms (Fig. 2). However, in $C_5I_5^+$ pronounced paratropic circulations are induced in the cyclopentadienyl unit, but no global circulations are found in I_5 unit. Similarly, in C_4I_4 strong paratropic currents circulate along the four-membered ring, while in $C_4I_4^{2+}$ relatively weak diatropic currents can be seen, except in the center of the ring that remain paratropic (Fig. 2). The π- and σ-electron current density maps of $C_5I_5^-$ and C_4I_4, and their oxidized forms provide a more detailed description of the magnetic aromaticity of these species (Fig. 3). The magnetic response of periodo-derivatives of cyclopentadienyl anion and cyclobutadiene, and their doubly oxidized products, can be understood using simple electron counting and Hückel's rule. In $C_5I_5^-$, 6 π-electrons and in C_4I_4, 4 π-electrons give rise to magnetic aromaticity and antiaromaticity, respectively. In both $C_5I_5^-$ and C_4I_4 the σ-electron molecular orbitals (MOs) are fully occupied with 10 and 8 electrons, respectively, and these electronic subsystems do not contribute to the global circulations (Fig. 3). A key difference between C_6I_6 on one hand, and C_4I_4 and $C_5I_5^-$ on the other, is that latter molecules feature a π-type HOMO level, while the former one has a σ-type HOMO (Fig. S1 and Table S1†). For this reason, upon oxidation to $C_5I_5^+$ and $C_4I_4^{2+}$ the number of π-electrons decreases by 2 compared to their non-oxidized forms, which explains the drastic change in π-aromaticity. Contrary, the number of σ-electrons stays unchanged in both species.

The oxidation effects on aromaticity in the studied molecules are found to be independent of the aromatic character of the parent, non-oxidized molecules (Fig. 2 and 3). The primary factor influencing magnetic properties is found to be the structural characteristic of the starting compounds. The examined molecules in their ground singlet state show various geometries: C_6I_6 and $C_6I_6^{2+}$ adopt planar D_{6h} geometries, $C_5I_5^-$

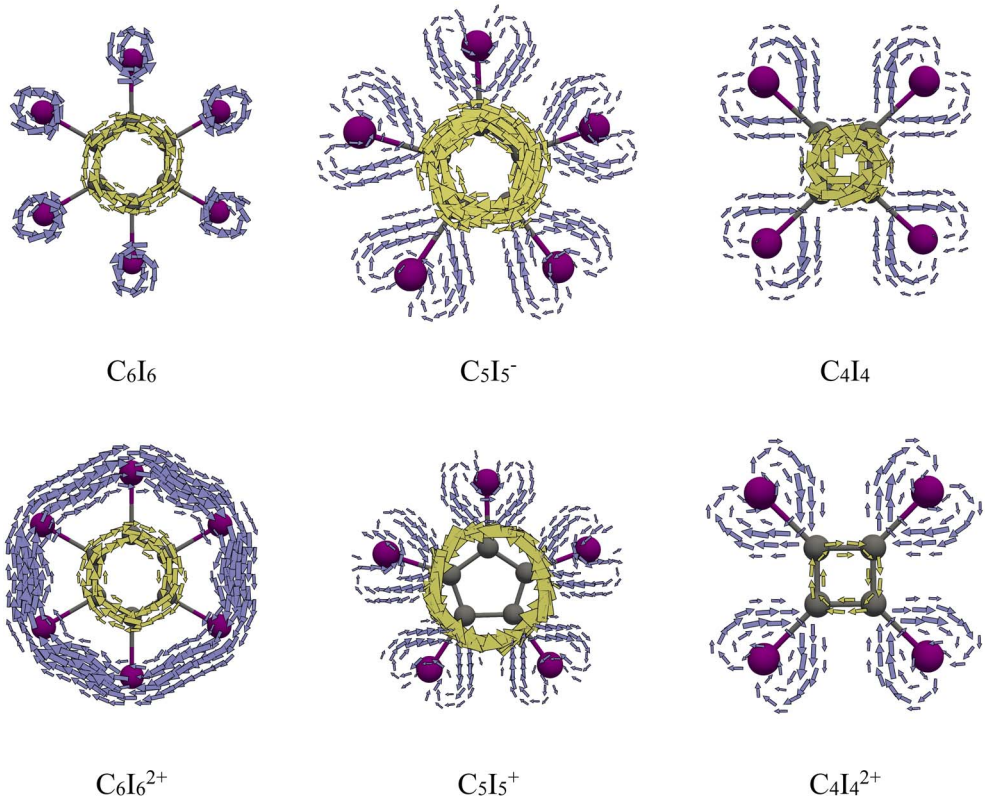

Fig. 3 π (yellow) and σ (purple) current density maps plotted 1 Bohr above molecular plane for C_6I_6, $C_6I_6^{2+}$, $C_5I_5^-$, $C_5I_5^+$, C_4I_4, and $C_4I_4^{2+}$.

adopts planar D_{5h} geometry, $C_5I_5^+$ adopts planar C_{2v} geometry, while C_4I_4 adopts D_{2h} geometry, and $C_4I_4^{2+}$ shows planar D_{4h} geometry in their ground singlet state (Fig. 1). Table 1 collects the iodine–iodine and carbon–carbon distances, along with the overlap integral values between the Pre-orthogonal Natural Bond Orbitals (PNBOs)[37] which depict the in-plane lone-pairs on I-atoms (Table 1 and Fig. S2†). As can be seen, the key structural feature influencing magnetic behavior upon oxidation is the size of carbon-atom ring. This factor ultimately determines the I–I distance, and consequently the overlap between the in-plane lone pair orbitals, which correspond to the 5p atomic orbitals on the iodine atoms (Fig. S3†). In C_6I_6 the I–I distance is 3.524 Å, while in the dication $C_6I_6^{2+}$ this distance decreases to 3.475 Å. This reduction of the I–I distances upon oxidation is followed by a decrease in the C–C bond lengths. As a result, the overlap of the in-plane lone pair orbitals on adjacent iodine atoms in $C_6I_6^{2+}$ is only slightly larger than that in C_6I_6. This suggests that significant overlap between the iodine in-plane lone pair orbitals is necessary for inducing σ-electron delocalization, but it is not the sole condition, as the number of σ-electrons also plays a crucial role. In the $C_5I_5^-$ anion, oxidation results in a substantial change in the C–C distances due to a complete reversal of aromaticity in the five-membered carbon ring. On the other hand, there is no significant change in the I–I distances, as well as in the overlap between the in-plane lone pair orbitals of iodine atoms. For C_4I_4 and its dication $C_4I_4^{2+}$, both C–C and I–I distances are reduced. However, the change in the I–I distance does not lead to any notable change in the overlap of specific orbitals in the iodine subunit, since the I–I distance remains above 4 Å, which prevents significant overlap of the iodine 5p orbitals.

Table 1 Bond lengths (in Å) for symmetry-unique C–C and I–I bonds and the absolute values of the overlap integral (S^{PNBO}) of in-plane lone pair PNBOs for C_6I_6, $C_6I_6^{2+}$, $C_5I_5^-$, $C_5I_5^+$, C_4I_4, and $C_4I_4^{2+}$

	C–C distance	I–I distance	S^{PNBO}
C_6I_6	1.405	3.524	0.124
$C_6I_6^{2+}$	1.389	3.475	0.129
C_4I_4	1.582	4.377	0.030
	1.329	4.333	0.032
$C_4I_4^{2+}$	1.450	4.269	0.026
$C_5I_5^-$	1.407	3.868	0.082
$C_5I_5^+$	1.448	3.812	0.070
	1.363	3.859	0.067
	1.534	3.837	0.066

The presented results show that the energy effect of mixing the in-plane lone pair orbitals on the iodine atoms, as indicated by the difference between the energies of the lowest and highest occupied σ-MOs (Table S1†), depends on the extent of the lone pair orbital overlap. Only when the overlap of the iodine 5p orbitals is sufficiently large does the energy of the highest occupied σ-MO, which has I–I antibonding character, become high enough to make this orbital the HOMO of the system from which electrons are removed in the oxidation process.

To provide more quantitative information on the induced current densities, an analysis based on the integrated current

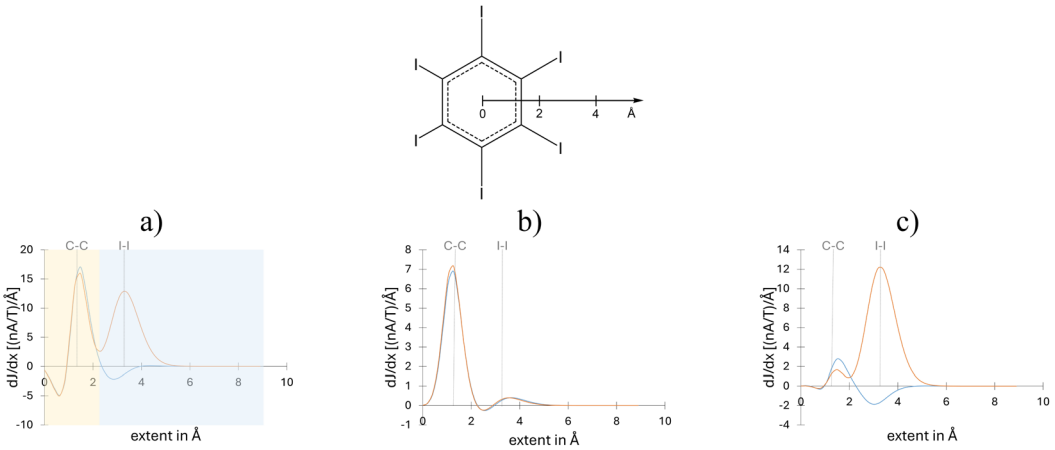

Fig. 4 Profiles of total (a), π (b), and σ (c) bond current strengths for C_6I_6 (blue line) and $C_6I_6^{2+}$ (orange line). The yellow and blue surfaces describe the integration areas used to separate the total current strength. Positive and negative current strengths correspond to diatropic and paratropic ring currents, respectively.

strengths was employed. For systems with a polycyclic structure, such as the studied molecules, the bond current strength profiles proved to be particularly insightful.[10] The advantage of the bond strength profiles is illustrated for C_6I_6 and its doubly oxidized cation (Fig. 4). The total bond current strength profiles of neutral C_6I_6 (blue line in Fig. 4a) reveal that inside the benzene ring (r < 1 Å) there are relatively weak paratropic currents, while outside the benzene ring, much stronger diatropic currents are observed, primarily arising from π-electron contributions. However, this contribution practically vanishes at approximately 2 Å from the ring center, where the effect of the σ-MOs of the I_6-system becomes dominant, although these MOs induce only weak paratropic circulations. On the other hand, for $C_6I_6^{2+}$ (orange line in Fig. 4a) two intensive peaks are found, corresponding to diatropic circulations around the carbon and around the iodine atom rings. The bond current strengths profiles dissected into π- and σ-electron contributions reveal that the oxidation of C_6I_6 causes a significant change in the magnetic response of the σ-electron system, while the π-electrons preserve their magnetic aromatic behavior. Bond current strengths profiles for $C_5I_5^-$ and C_4I_4, as well as for their oxidized forms are provided in the ESI (Fig. S4 and S5†).

As illustrated for $C_6I_6^{2+}$ (Fig. 4a), the profile curve can be used to define an integration surface that allows for the division of the total currents into contributions from two circulations: one around the benzene ring and the other around the iodine atom ring. Using this approach, the total current strengths for all studied molecules were dissected into contribution from the carbon atom ring and the outer iodine atom ring. For the bond current strengths of both π- and σ-electrons, the integration surface was not separated, but rather used to the entire integration area. The bond current strengths calculated in this way for periodo-monocyclic molecules are collected in Table 2, along with the corresponding EDDB and I_{ring} values. The EDDB values were further decomposed into their π- and σ-electron contributions.

Before proceeding, it should be noted that the aromaticity indices for $C_6I_6^{2+}$ were also obtained using different density functionals and basis sets (Table S2†). The comparison shows that the choice of functional and the size of the basis set have only a minor impact on the numerical values of the aromaticity indices, in agreement with a previous study.[10] The largest difference is observed in the bond current strength for the I_6

Table 2 Calculated bond current strengths (J, in nA T^{-1}), EDDB (in a.u.), and I_{ring} (in a.u.) values for the studied monocyclic molecules. The numbers in parentheses represent the total number of electrons

		J [nA T^{-1}]	$EDDB_F$	I_{ring}	J^{π} [nA T^{-1}]	$EDDB_{\pi}$	J^{σ}[nA T^{-1}]	$EDDB_{\sigma}$
C_6I_6	C_6	9.4	5.074	0.627	6.4	5.737 (6)	−2.0	0.623 (12)
	I_6	−1.0	0.227	0.066				
$C_6I_6^{2+}$	C_6	8.6	5.038	0.624	6.6	5.733 (6)	17.6	5.812 (10)
	I_6	18.7	5.333	0.310				
$C_5I_5^-$	C_5	9.4	5.470	0.617	8.3	5.569 (6)	−0.2	0.416 (10)
	I_5	0.2	0.108	−0.042				
$C_5I_5^+$	C_5	−92.8	1.236	0.478	−83	2.164 (4)	−0.2	0.695 (10)
	I_5	−0.7	0.529	−0.092				
C_4I_4	C_4	−12.3	0.211	0.216	−8.6	0.719 (4)	0.5	0.558 (8)
	I_4	0.5	0.073	0.075				
$C_4I_4^{2+}$	C_4	−1.9	1.225	0.459	1.8	1.451 (2)	0.5	0.698 (8)
	I_4	0.6	0.064	0.055				

unit, which is partly due to the practical challenge of accurately separating the currents circulating along the C_6 and I_6 rings.

As can be observed from the bond current strengths, the induced currents along the I_6 ring in the dication $C_6I_6^{2+}$ are significantly stronger than those along the benzene ring. For C_6I_6, both EDDB and I_{ring} values indicate a significant increase in electron delocalization within the I_6 ring upon oxidation. Additionally, these indices confirm that in all parent (non-oxidized) molecules no cyclic delocalization occurs within the iodine atom units. Furthermore, the electronic indices show that the oxidation of $C_5I_5^-$ and C_4I_4 does not affect the (non) aromatic character of the iodine atom rings. Contrary to predictions based on the bond current strengths, EDDB and I_{ring} values suggest that the cyclic delocalization in the I_6 unit of $C_6I_6^{2+}$ is significantly weaker than that in the benzene fragment (Table 2). In particular, the I_{ring} values predict that the aromaticity of the I_6 ring is approximately half of that in the benzene ring. Similarly, in $C_6I_6^{2+}$ the $EDDB_\pi$ value is 5.737 (out of 6 electrons), while the $EDDB_\sigma$, which describes electron delocalization within the I_6 ring, is 5.812 (out of 10 electrons). As can be seen from the EDDB surfaces presented in Fig. 5, π-electrons are delocalized in C_6I_6, $C_6I_6^{2+}$, $C_5I_5^-$, and $C_4I_4^{2+}$, while σ-electrons are delocalized only in $C_6I_6^{2+}$.

To further investigate the significance of σ-aromaticity and to isolate its effects from those of π-electron aromaticity, we also examined periodo-borazine (Fig. S6†). It is worth noting that the aromaticity of borazine has been the subject of considerable debate.[38–40] Magnetic and energetic criteria have generally characterized borazine as weakly π-aromatic.[41] Similarly, the bond current strengths suggest that $B_3N_3I_6$ is π-nonaromatic, while electronic indices predict relatively weak π-aromatic character (Fig. S7 and Table S3†). Both magnetic and electronic descriptors indicate that the oxidized species, $B_3N_3I_6^{2+}$, exhibits pronounced σ-electron aromaticity, in agreement with a recent study.[42] The oxidation of neutral $B_3N_3I_6$ to $B_3N_3I_6^{2+}$ induces σ-aromaticity, which is clearly reflected in its structural properties: a reduction in I–I distances and planarization of the molecule (Fig. S6†). Notably, σ-electron aromaticity in $B_3N_3I_6^{2+}$ completely annuls the distortive effect of the I-substituents. It is important to emphasize that the observed structural features are characteristic signatures of aromaticity and, more importantly, are readily accessible through experimental observation.

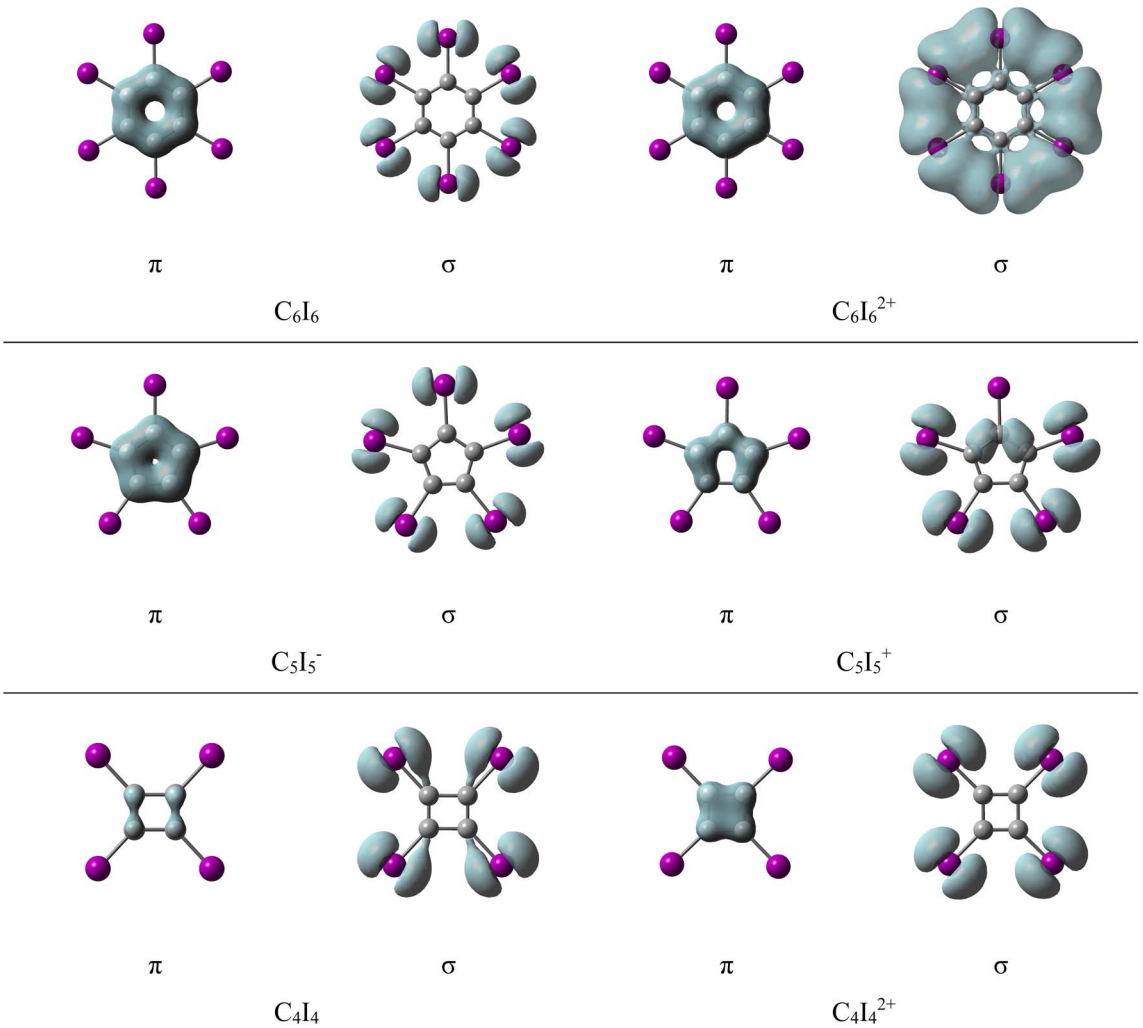

Fig. 5 Isosurface of the $EDDB_H$ function calculated for π-electrons (isovalue of 0.01 a.u.) and for σ-electrons (isovalue 0.001 a.u.).

Periodo-polycyclic (anti)aromatic hydrocarbons

The study of periodo-derivatives of monocyclic conjugated hydrocarbons, as outlined above, clearly demonstrated that the main factor influencing the occurrence of oxidation induced σ-aromaticity is the size of the carbon atom rings. This structural factor determines the distance between iodine atoms, and consequently the overlap of their in-plane lone pair orbitals. Additionally, the number of σ-electrons is another factor that plays a crucial role in determining the σ-electron aromatic properties. This accumulated knowledge provides a solid foundation for exploring potential double aromaticity in periodo-derivatives of polycyclic (anti)aromatic hydrocarbons and their oxidized species. To begin, periodo-derivatives of bicyclic hydrocarbons such as pentalene and naphthalene are

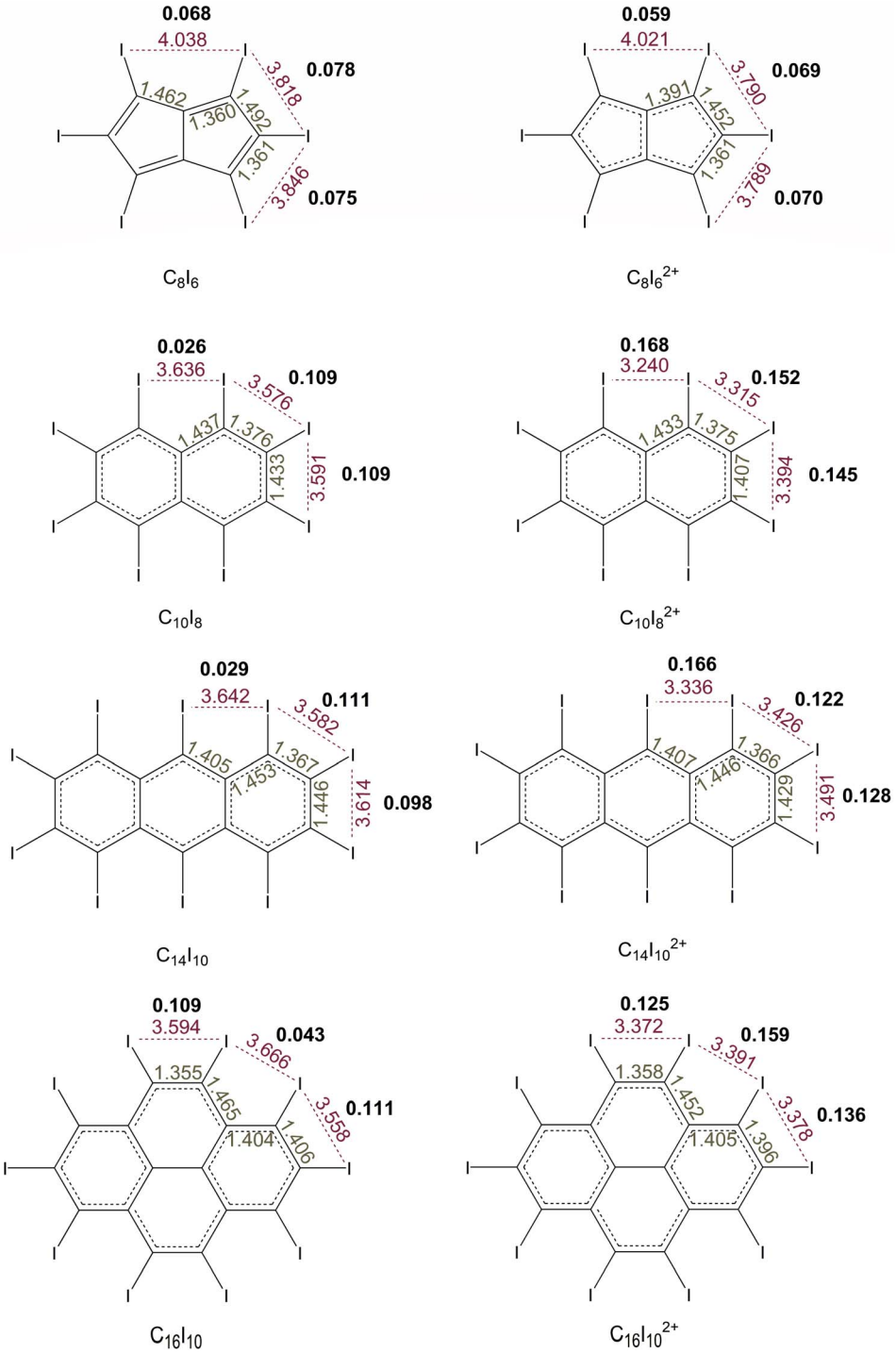

Fig. 6 The absolute values of the overlap integral values of in-plane lone pair PNBOs (bold numbers), along with the C–C and I–I distances (in Å) for symmetry-unique bonds in C_8I_6, $C_8I_6^{2+}$, $C_{10}I_8$, $C_{10}I_8^{2+}$, $C_{14}I_{10}$, $C_{14}I_{10}^{2+}$, $C_{16}I_{10}$, and $C_{16}I_{10}^{2+}$.

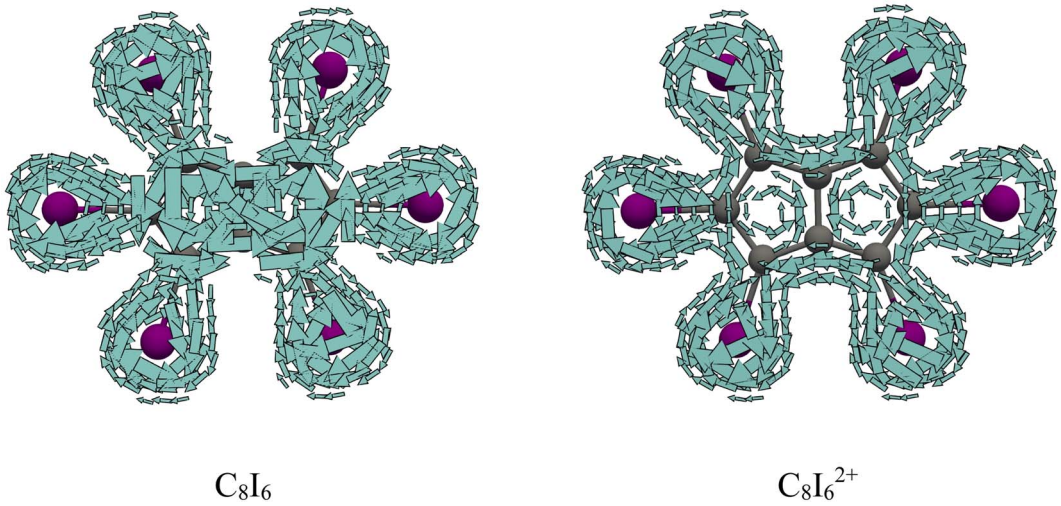

Fig. 7 Total current density maps plotted 1 Bohr above the molecular plane for C_8I_6 and $C_8I_6^{2+}$ (a) and (b).

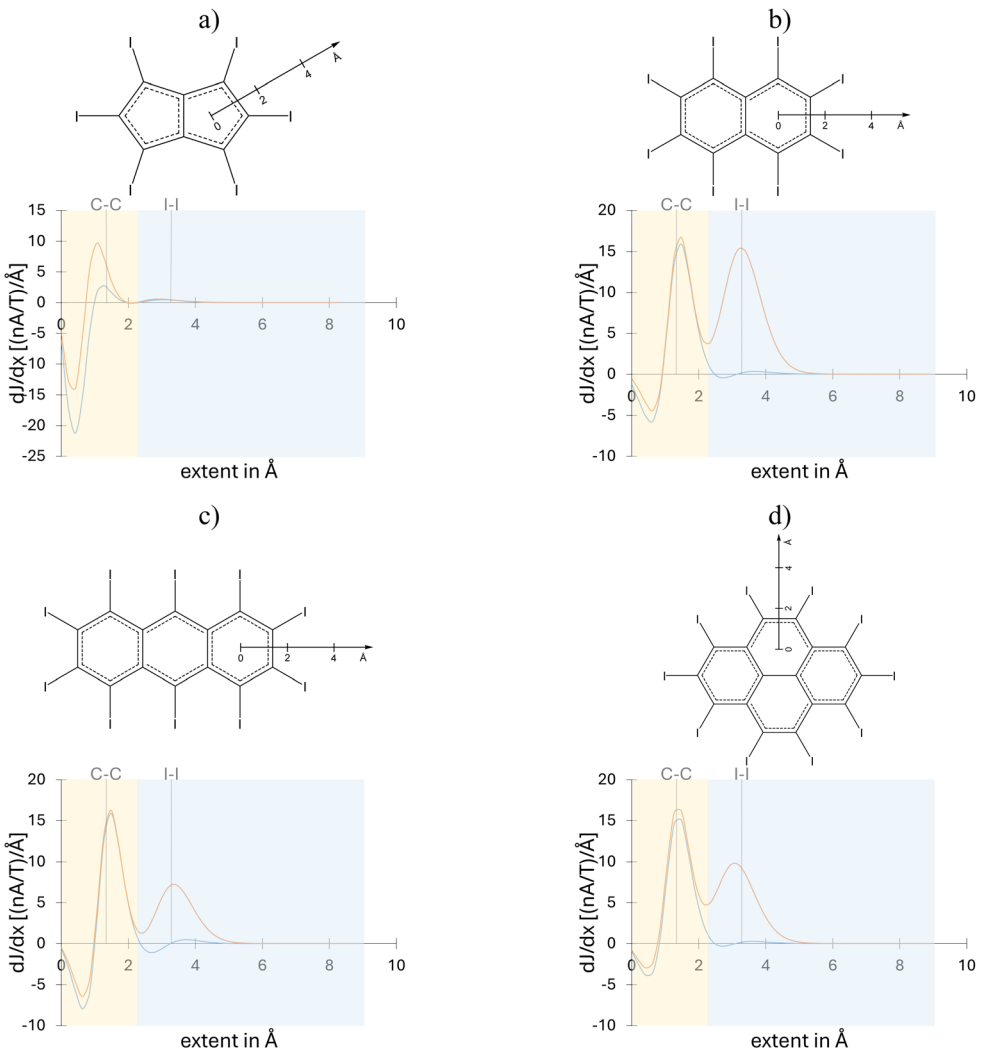

Fig. 8 Total bond current strengths profiles of C_8I_6 (blue line) and $C_8I_6^{2+}$ (orange line) (a); $C_{10}I_8$ (blue line) and $C_{10}I_8^{2+}$ (orange line) (b); $C_{14}I_{10}$ (blue line) and $C_{14}I_{10}^{2+}$ (orange line) (c); $C_{16}I_{10}$ (blue line) and $C_{16}I_{10}^{2+}$ (orange line) (d).

explored, before expanding the series to include periodo-derivatives of anthracene and perylene.

Periodo-pentalene (C_8I_6) adopts planar C_{2h}, while periodo-pentalene dication ($C_8I_6^{2+}$) adopts D_{2h} geometry in their ground singlet state (Fig. 1). On the other hand, all other polycyclic periodo-derivatives exhibit nonplanar geometries with reduced symmetries. For this reason, in what follows aromaticity indices were not dissected into σ/π contributions. The critical atom distances and the overlap of the in-plane lone pair orbitals on neighboring iodine atoms are presented in Fig. 6. The structural features of the five-membered rings within the pentalene unit have a significant impact on the distances between iodine atoms. In C_8I_6 the I–I distance ranges from 3.818 to 4.038 Å, while in $C_8I_6^{2+}$ this distance is only slightly reduced to 3.780–4.021 Å. These distances, and consequently the overlap of the iodine 5p atomic orbitals, are similar to those observed in $C_5I_5^-$ and $C_5I_5^+$. The small change in the I–I distance upon oxidation does not lead to any substantial alternation in the overlap of the iodine 5p atomic orbitals. Thus, it is not likely to expect any significant cyclic electron delocalization in the I_6 unit of $C_8I_6^{2+}$. Indeed, the current density maps (Fig. 7) and profiles of the integrated current density (Fig. 8) for C_8I_6 show pronounced paratropic currents within the pentalene unit, while for $C_8I_6^{2+}$, these currents become weak and diatropic. In both molecules, only local currents are induced around the iodine atoms. As shown for C_6I_6 (Fig. 4), the current strength profiles of C_8I_6 and $C_8I_6^{2+}$ were used to extract the information on the strength of the current density circulations around the carbon and iodine atom rings (Table 3). The current strength profiles for periodo-pentalene resemble those of periodo-cyclobutadiene. The current density profile for neutral C_8I_6 is dominated by a negative peak, corresponding to paratropic currents along the pentalene unit (Fig. 8). In $C_8I_6^{2+}$, these paratropic currents are significantly reduced, indicating an overall diatropic character, while there is no evidence of σ-electron currents around the I_6 macrocycle (Fig. 8). These results can be explained in a similar manner to C_4I_4: upon oxidation, the number of π-electrons changes from 8 to 6 (the HOMO of pentalene is relatively high in energy as expected from an antiaromatic molecule), while the number of σ-electrons remains constant. Because, in general, the HOMO of antiaromatic species is of π-character, we expect that such systems will not show double (anti)aromaticity after oxidation. The EDDB and I_{ring} values agree with the current density analysis regarding the aromaticity of the I_6 unit in both C_8I_6 and its oxidized form (Table 3). However, the EDDB does not predict such a significant change in the aromaticity of the pentalene unit when going from C_8I_6 to $C_8I_6^{2+}$. On the other hand, the I_{ring} predicts an unreasonably high delocalization within the pentalene unit in both C_8I_6 and $C_8I_6^{2+}$. Overall, the electronic aromaticity indices are inadequate for accurate differentiation between antiaromatic and nonaromatic species in periodo-pentalene.

The periodo-naphthalene ($C_{10}I_8$) and periodo-naphthalene dication ($C_{10}I_8^{2+}$) have nonplanar D_2 geometry. The extent of their nonplanarity was evaluated using the BFPI (brute-force planarity index)[43] (Table 3). In $C_{10}I_8$, the distance between

Table 3 Calculated BFPI values, bond current strengths (J, in nA T^{-1}), EDDB (in a.u.), and I_{ring} (in a.u.) values for periodo-derivatives of polycyclic (anti)aromatic hydrocarbons

	BFPI [Å]		J [nA T^{-1}]	EDDB	I_{ring}
C_8I_6	0.000	C_8	−14.8	2.511	0.517
		I_6	0.5	0.214	0.040
$C_8I_6^{2+}$	0.000	C_8	3.1	4.481	0.546
		I_6	1.0	0.530	−0.052
$C_{10}I_8$	6.779	C_{10}	8.6	5.918	0.575
		I_8	0.3	0.252	0.080
$C_{10}I_8^{2+}$	2.772	C_{10}	10.5	7.085	0.592
		I_8	21.4	5.825	0.204
$C_{14}I_{10}$	9.466	C_{14}	6.4	8.130	0.557
		I_{10}	−0.2	0.301	0.068
$C_{14}I_{10}^{2+}$	7.554	C_{14}	8.3	8.916	0.571
		I_{10}	9.6	6.089	0.141
$C_{16}I_{10}$	9.079	C_{16}	10.2	7.233	0.545
		I_{10}	0.1	0.266	0.087
$C_{16}I_{10}^{2+}$	7.318	C_{16}	13.7	7.656	0.562
		I_{10}	12.9	6.146	0.155

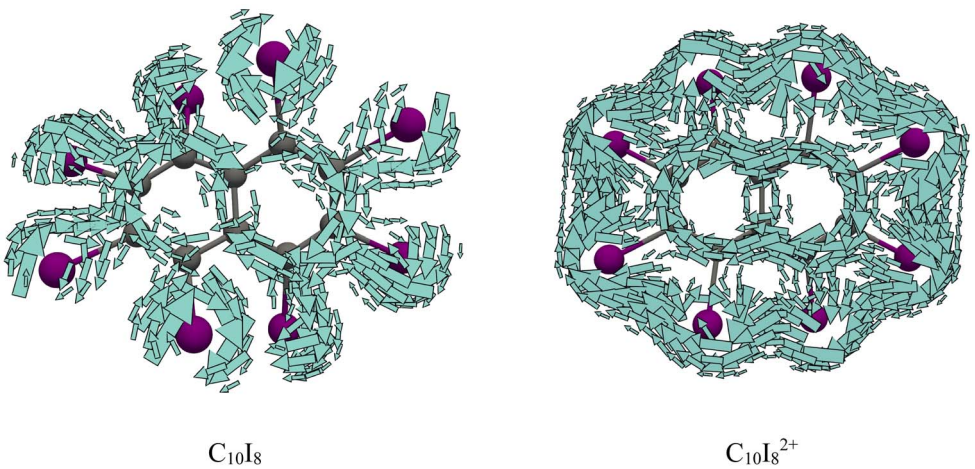

Fig. 9 Total current density maps plotted 1 Bohr above the molecular plane for $C_{10}I_8$ and $C_{10}I_8^{2+}$.

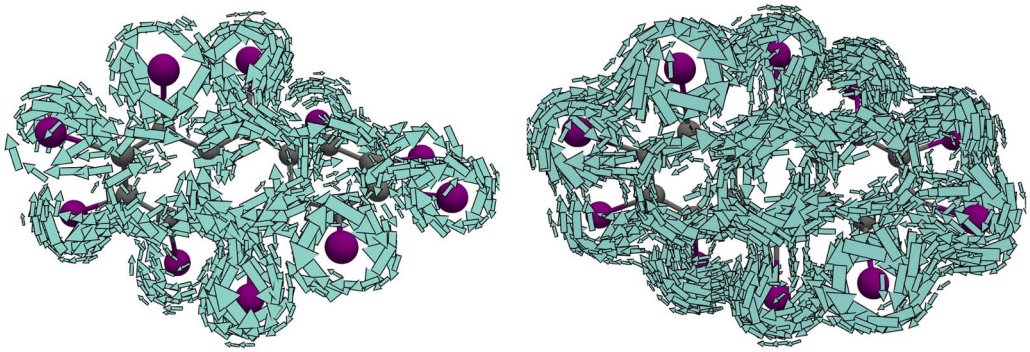

$C_{14}I_{10}$ $C_{14}I_{10}^{2+}$

Fig. 10 Total current density maps plotted 1 Bohr above the molecular plane for $C_{14}I_{10}$ and $C_{14}I_{10}^{2+}$.

iodine atoms ranges from 3.576 to 3.636 Å, whereas in $C_{10}I_8^{2+}$ these distances are significantly shortened. This reduction is especially pronounced for the distance between the two I atoms in the α-positions on the adjacent hexagons, which decreases from 3.636 Å to 3.240 Å. Consequently, upon oxidation, the overlap of the corresponding iodine 5p atomic orbitals drastically increases from 0.026 to 0.168 (Fig. 6). The contraction in I–I distance is much more pronounced than that found during the oxidation of C_6I_6 (Table 1). The BFPI nonplanarity index further shows that oxidation of $C_{10}I_8$ enhances planarity of the corresponding product. This feature is already evident in the side-view geometries of these two species (Fig. 1). Current density maps and profiles of current density strengths of the $C_{10}I_8^{2+}$ dication (Fig. 8 and 9) reveal its double aromatic nature. In $C_{10}I_8^{2+}$, diatropic currents are induced along the perimeter formed by the iodine atoms, while there are no such currents in neutral $C_{10}I_8$. In both $C_{10}I_8$ and $C_{10}I_8^{2+}$ the current density distribution in the naphthalene unit resembles that in naphthalene itself. The integrated current strengths for circulations along the carbon and iodine atom rings are 10.5 and 21.5 nA T^{-1}, respectively. According to the magnetically induced current density, both the naphthalene and macrocycle I_8 units of the $C_{10}I_8^{2+}$ dication display significant aromatic character despite distortions in planarity. These findings are generally supported by the EDDB and I_{ring} values. Based on the magnetic and electronic indices, oxidation of $C_{10}I_8$ induces σ-aromaticity, while the resulting $C_{10}I_8^{2+}$ dication gains additional planarity and enhanced aromaticity in the naphthalene unit in comparison to the neutral molecule. The $C_{10}I_8^{2+}$ dication is a double Hückel 4n + 2 system, with 10 π-electrons and 14 σ-electrons. To further evaluate the effect of halogen lone-pair orbital overlap on oxidation induced σ-aromaticity, $C_{10}Br_8$ and $C_{10}Br_8^{2+}$ were also included in this study (Fig. S8†). Oxidation of $C_{10}Br_8$ to $C_{10}Br_8^{2+}$ results in shorter Br–Br distances and enhanced overlap of Br lone pair orbitals. Due to the smaller van der Waals radius of bromine compared to iodine, $C_{10}Br_8^{2+}$ adopts a fully planar geometry, allowing more significant overlap of the corresponding in-plane lone pair orbitals on the two Br atoms in the α-positions on the adjacent hexagons. Both magnetic and electronic indices predict considerable σ-electron delocalization in $C_{10}Br_8^{2+}$, although slightly less intense than in $C_{10}I_8^{2+}$ (Fig. S9 and Table S4†). However, a more detailed investigation into how the nature of halogen substituents influences oxidation-induced σ-aromaticity in polycyclic molecules remains a task for future studies.

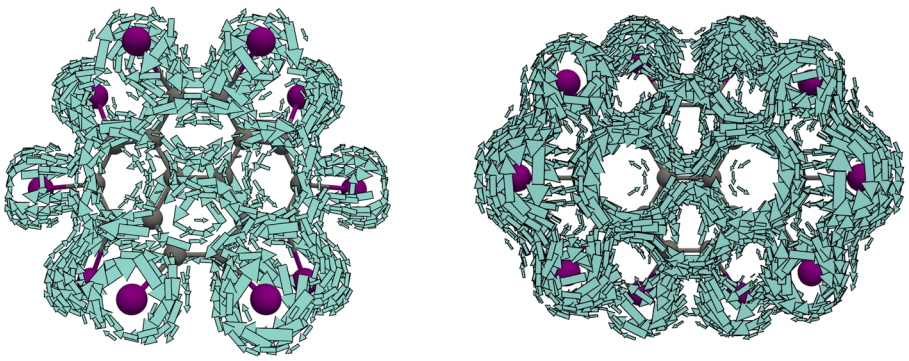

$C_{16}I_{10}$ $C_{16}I_{10}^{2+}$

Fig. 11 Total current density maps plotted 1 Bohr above the molecular plane for $C_{16}I_{10}$ and $C_{16}I_{10}^{2+}$.

The periodo-anthracene ($C_{14}I_{10}$) exhibits C_1 symmetry, periodo-anthracene dication ($C_{14}I_{10}^{2+}$) adopts nonplanar D_2 geometry, while the periodo-perylene ($C_{16}I_{10}$) and periodo-perylene dication ($C_{16}I_{10}^{2+}$) have nonplanar C_{2v} geometry (Fig. 1). In $C_{14}I_{10}$, the distance between iodine atoms ranges from 3.582 to 3.642 Å, while in $C_{14}I_{10}^{2+}$ this distance decreases notably to 3.336–3.491 Å (Fig. 6). The I–I distance shortening is accompanied by a substantial increase of the overlap of the iodine lone pair orbitals (Fig. 6). Similarly, the oxidation of $C_{16}I_{10}$ to $C_{16}I_{10}^{2+}$ leads to a reduction of I–I distances and to an enhanced overlap of the 5p iodine orbitals. Both $C_{14}I_{10}^{2+}$ and $C_{16}I_{10}^{2+}$ adopt more planar structure compared to their non-oxidized forms (Table 3 and Fig. 1). Based on these observations, one can anticipate that the double oxidation of $C_{14}I_{10}$ and $C_{16}I_{10}$ will induce σ-electron delocalization within the I_{10} units of the corresponding oxidation products (Fig. 8, 10, and 11).

Current density maps and integrated current density profiles for neutral $C_{14}I_{10}$ and $C_{16}I_{10}$ reveal the aromatic characteristics of the anthracene and perylene units, despite notable geometric distortions in these molecules (Table 3 and Fig. 1), and additionally, no evidence of any global σ-electron current density circulations. Similar to the periodo-naphthalene dication, the magnetically induced currents support the presence of double aromaticity in the $C_{14}I_{10}^{2+}$ and $C_{16}I_{10}^{2+}$ molecules. The

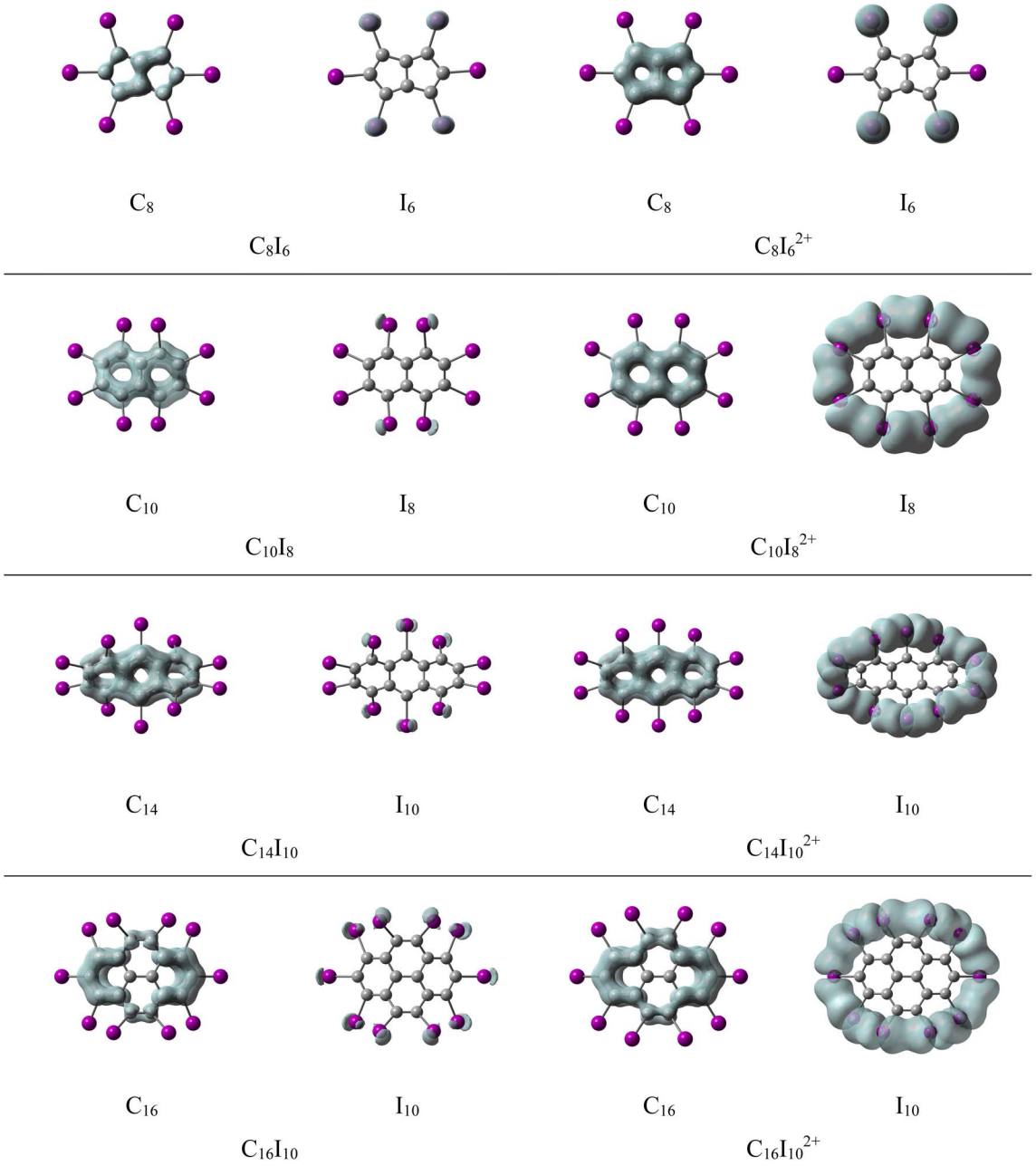

Fig. 12 Isosurfaces of the $EDDB_F$ function calculated for the C-atom units (isovalue of 0.01 a.u.) and for the I-atom units (isovalue of 0.001 a.u.) in the considered molecules.

Table 4 Zero-point (Δ_rZPE) and Gibbs ($\Delta_r G$) reaction energies (kcal mol^{-1}) for selected homodesmotic reactions

	Δ_rZPE	$\Delta_r G$
$C_6I_6^{2+} + C_6I_5H \rightarrow C_6I_5H^{2+} + C_6I_6$	23.2	22.6
$C_{10}I_8^{2+} + C_{10}I_7H \rightarrow C_{10}I_7H^{2+} + C_{10}I_8$	6.0	6.2
$C_{14}I_{10}^{2+} + C_{14}I_9H \rightarrow C_{14}I_9H^{2+} + C_{14}I_{10}$	2.9	2.9
$C_{16}I_{10}^{2+} + C_{16}I_9H \rightarrow C_{16}I_9H^{2+} + C_{16}I_{10}$	5.0	5.3

integrated bond current strengths suggest that the σ-electron currents within the I_{10} macrocyclic are more intensive in $C_{16}I_{10}^{2+}$ than in $C_{14}I_{10}^{2+}$ (Fig. 8 and Table 3). This goes in line with the obtained EDDB and I_{ring} values (Table 3). Even though periodo-anthracene and periodo-perylene dications are highly nonplanar, significant overlap between the lone pair orbitals on the iodine atoms facilitates cyclic σ-electron delocalization, which is evident from both the magnetic and electronic aromaticity indices. EDDB surfaces presented in Fig. 12 further confirm double aromatic character in $C_{10}I_8^{2+}$, $C_{14}I_{10}^{2+}$, and $C_{16}I_{10}^{2+}$.

As discussed above, both magnetic and electronic aromaticity indices consistently indicate that double oxidation of periodo-derivatives of naphthalene, anthracene, and perylene induces σ-electron delocalization within the I-containing macrocycles of the corresponding oxidation products. Furthermore, the presence of σ-aromaticity in the oxidized species should be readily observable experimentally, as these molecules exhibit shorter I–I distances and increased planarity compared to their non-oxidized forms (Fig. 1 and 6). A generally good correlation is observed between the shortening of I–I distances, enhanced overlap of iodine 5p atomic orbitals, and the increase in aromaticity indices upon oxidation in studied molecules (Fig. S10†).

Finally, we investigated the energetic aspect of oxidation induced σ-electron aromaticity using carefully designed homodesmotic reactions (Table 4). It is important to note that the selected reactions differ somewhat from those employed in recent work by some of the present authors.[12,13] This adjustment was made to provide a more balanced treatment of planarity distortions between reactants and products. Further details regarding these reactions are provided in Fig. S11.† As shown in Table 4, the stabilization effects of σ-electron aromaticity decrease rapidly with increasing size of the I-macrocycle, in agreement with previous studies.[44,45] Additionally, the relatively modest stabilization effects can be partly attributed to significant deviations from planarity within the σ-electron system.

Conclusions

In this study, the aromatic character of a series of periodo-derivatives of monocyclic and polycyclic (anti)aromatic hydrocarbons, along with their doubly oxidized forms, was investigated using electronic (I_{ring} and EDDB), magnetic (MICD) and energetic (aromatic stabilization energy) indicators. The analysis of periodo-derivatives of monocyclic conjugated hydrocarbons clearly demonstrated that the primary factor influencing the appearance of oxidation-induced σ-aromaticity is the size of the carbon atom rings. This structural feature was found to govern the distance between iodine atoms, which, in turn, determinates the overlap of their in-plane lone pair orbitals. Only when the overlap of the iodine 5p orbitals becomes sufficiently large, the highest occupied σ-molecular orbital, can become the HOMO, from which electrons are removed during the oxidation process. Furthermore, it was found that the number of σ-electrons is another factor that plays a crucial role in determining the σ-electron aromaticity of the corresponding oxidized structures.

Based on this knowledge, potential double aromaticity in periodo-derivatives of polycyclic (anti)aromatic hydrocarbons was further explored. It was found that the oxidation of periodopentalene does not induce σ-electron delocalization in the iodine macrocyclic ring, as only the number of π-electrons is altered during this process. On the other hand, for periodo-derivatives of naphthalene, anthracene, and perylene, the oxidation was found to enhance planarity of the corresponding products, along with a significant increase in the overlap of the iodine 5p atomic orbitals. Both magnetic and electronic aromaticity indices revealed the presence of σ-aromaticity in the iodine macrocyclic rings and, more importantly, the double aromatic character of the oxidized forms of these molecules.

Computational methods

Geometry optimizations and vibrational frequency calculations for all studied molecules were performed at the B3LYP/def2-TZVP[46–49] level of theory using Gaussian 09 program package.[50] The magnetically induced current density (MICD) was calculated at the same level of theory, using the diamagnetic zero (DZ) version of the CTOCD method.[51–54] The MICD was calculated by applying the external magnetic field oriented perpendicular to the molecular planes. In the MICD maps, clockwise circulations denote diatropic currents, while counterclockwise circulations indicate paratropic currents. The maps were generated using the ParaView software.[55] The current strengths (J, in nA T^{-1})[56] were obtained by numerical integration of the current densities passing through a rectangle which perpendicularly bisects the considered bond. The integration rectangle extends 5 Bohr above and 5 Bohr below the molecular plane, and it starts from the ring center and extends 15 Bohr outside the C-atom ring, to take into account all currents induced along the I-atom subunits. Diatropic (paratropic) currents give positive (negative) contributions to the current strength.

The multicenter index I_{ring} was calculated using the natural atomic orbital (NAO) density matrices obtained from NBO analysis.[37] The I_{ring} values were normalized based on the ring's size.[57]

To assess the reliability of the B3LYP/def2-TZVP results, a set of test calculations for C_6I_6 and $C_6I_6^{2+}$ was performed with three different density functionals (CAM-B3LYP,[58] BP86,[59,60] ωB97XD[61]) and two additional basis sets (def2-SVP and def2-TZVPPD).

The aromatic stabilization energy[34,35] was calculated through a set of properly designed homodesmotic reactions.

The extent of the deviation from planarity for the examined molecules was quantified by means of the brute-force planarity index (BFPI).[43] The BFPI presents the average distance of all atoms from the optimal plane, obtained by minimizing that distance in the given molecule.

MICD, I_{ring}, and BFPI were calculated using in-house FORTRAN codes, while the EDDB values were calculated using the RunEDDB code.[62]

Data availability

The data supporting this article have been included as part of the ESI.†

Author contributions

The manuscript was written through contributions of all authors. All authors have given approval to the final version of the manuscript.

Conflicts of interest

There are no conflicts to declare.

Acknowledgements

S. R. and S. Đ. would like to dedicate this paper to students and teachers who stood against corruption and the collapse of the educational system in Serbia during the 2024–2025 academic year. S. Đ. and S. R. thank the Serbian Ministry of Science, Technological Development, and Innovation (Agreement No. 451-03-137/2025-03/200122). J. P. and M. S. thank the Spanish Ministerio de Ciencia, Innovación y Universidades (MCIN/AEI/10.13039/501100011033, projects: PID2023-147424NB-I00, PID2022-138861NB-I00, and CEX2021-001202-M) and the Generalitat de Catalunya (projects: 2021SGR442 and 2021SGR623 and ICREA Academia 2024 Prize to M. S.).

References

1 M. J. S. Dewar, *Bull. Soc. Chim. Belg.*, 1979, **88**, 957–967.
2 D. Cremer, *Tetrahedron*, 1988, **44**, 7427–7454.
3 R. W. A. Havenith, F. De Proft, P. W. Fowler and P. Geerlings, *Chem. Phys. Lett.*, 2005, **407**, 391–396.
4 J. Chandrasekhar, E. D. Jemmis and P. von R. Schleyer, *Tetrahedron Lett.*, 1979, **20**, 3707–3710.
5 E. D. Nelson and H. I. Kenttämaa, *J. Am. Soc. Mass Spectrom.*, 2001, **12**, 258–267.
6 D. J. Sagl and J. C. Martin, *J. Am. Chem. Soc.*, 1988, **110**, 5827–5833.
7 S. Furukawa, M. Fujita, Y. Kanatomi, M. Minoura, M. Hatanaka, K. Morokuma, K. Ishimura and M. Saito, *Commun. Chem.*, 2018, **1**, 60.
8 I. Ciofini, P. P. Lainé and C. Adamo, *Chem. Phys. Lett.*, 2007, **435**, 171–175.
9 R. W. A. Havenith, P. W. Fowler, S. Fias and P. Bultinck, *Tetrahedron Lett.*, 2008, **49**, 1421–1424.
10 M. Rauhalahti, S. Taubert, D. Sundholm and V. Liégeois, *Phys. Chem. Chem. Phys.*, 2017, **19**, 7124–7131.
11 S. Escayola, N. Proos Vedin, A. Poater, H. Ottosson and M. Solà, *J. Phys. Org. Chem.*, 2023, **36**, e4447.
12 J. Poater, S. Escayola, A. Poater, F. Teixidor, H. Ottosson, C. Viñas and M. Solà, *J. Am. Chem. Soc.*, 2023, **145**, 22527–22538.
13 J. Poater, S. Escayola, A. Poater, F. Teixidor, H. Ottosson, C. Viñas and M. Solà, *J. Am. Chem. Soc.*, 2025, **147**, 2914.
14 P. W. Fowler and R. W. A. Havenith, *J. Phys. Chem. A*, 2021, **125**, 6374–6383.
15 J. Barroso, S. Pan and G. Merino, *Chem. Soc. Rev.*, 2022, **51**, 1098–1123.
16 S. Đorđević and S. Radenković, *Phys. Chem. Chem. Phys.*, 2022, **24**, 5833–5841.
17 S. Đorđević and S. Radenković, *ChemPhysChem*, 2022, **23**, e202200070.
18 P. W. Fowler, N. Mizoguchi, D. E. Bean and R. W. A. Havenith, *Chem.–Eur. J.*, 2009, **15**, 6964–6972.
19 D. E. Bean, P. W. Fowler and A. Soncini, *Chem. Phys. Lett.*, 2009, **483**, 193–197.
20 A. J. Stasyuk, O. A. Stasyuk, M. Solà and A. A. Voityuk, *Chem. Commun.*, 2020, **56**, 352–355.
21 G. V Baryshnikov, R. R. Valiev, A. V Kuklin, D. Sundholm and H. Ågren, *J. Phys. Chem. Lett.*, 2019, **10**, 6701–6705.
22 G. V Baryshnikov, R. R. Valiev, R. T. Nasibullin, D. Sundholm, T. Kurten and H. Ågren, *J. Phys. Chem. A*, 2020, **124**, 10849–10855.
23 G. V Baryshnikov, R. R. Valiev, L. I. Valiulina, A. E. Kurtsevich, T. Kurtén, D. Sundholm, M. Pittelkow, J. Zhang and H. Ågren, *J. Phys. Chem. A*, 2022, **126**, 2445–2452.
24 K. Kaiser, L. M. Scriven, F. Schulz, P. Gawel, L. Gross and H. L. Anderson, *Science*, 2019, **365**, 1299–1301.
25 H. Li, R. Parida, S. Mukamel and J. Y. Lee, *Phys. Chem. Chem. Phys.*, 2024, **26**, 10284–10288.
26 I. Rončević, F. J. Leslie, M. Rossmannek, I. Tavernelli, L. Gross and H. L. Anderson, *J. Am. Chem. Soc.*, 2023, **145**, 26962–26972.
27 Y. Lyu, Y. Cui, H. Xu, C. Zhang and Q. Meng, *J. Org. Chem.*, 2024, **89**, 18244–18254.
28 M. Giambiagi, M. S. de Giambiagi, C. D. dos Santos Silva and A. P. de Figueiredo, *Phys. Chem. Chem. Phys.*, 2000, **2**, 3381–3392.
29 D. W. Szczepanik, *Comput. Theor. Chem.*, 2016, **1080**, 33–37.
30 D. W. Szczepanik, M. Andrzejak, J. Dominikowska, B. Pawełek, T. M. Krygowski, H. Szatylowicz and M. Solà, *Phys. Chem. Chem. Phys.*, 2017, **19**, 28970–28981.
31 P. Lazzeretti, *Phys. Chem. Chem. Phys.*, 2004, **6**, 217–223.
32 D. Sundholm, H. Fliegl and R. J. F. Berger, *Wiley Interdiscip. Rev.: Comput. Mol. Sci.*, 2016, **6**, 639–678.
33 D. Sundholm, M. Dimitrova and R. J. F. Berger, *Chem. Commun.*, 2021, **57**, 12362–12378.
34 S. W. Slayden and J. F. Liebman, *Chem. Rev.*, 2001, **101**, 1541–1566.
35 M. K. Cyrański, *Chem. Rev.*, 2005, **105**, 3773–3811.
36 M. Solà, *Nat. Chem.*, 2022, **14**, 585–590.

37 J. P. Foster and F. Weinhold, *J. Am. Chem. Soc.*, 1980, **102**, 7211–7218.
38 D. Benker, T. M. Klapötke, G. Kuhn, J. Li and C. Miller, *Heteroat. Chem.*, 2005, **16**, 311–315.
39 J. J. Engelberts, R. W. A. Havenith, J. H. van Lenthe, L. W. Jenneskens and P. W. Fowler, *Inorg. Chem.*, 2005, **44**, 5266–5272.
40 R. Islas, E. Chamorro, J. Robles, T. Heine, J. C. Santos and G. Merino, *Struct. Chem.*, 2007, **18**, 833–839.
41 R. Báez-Grez and R. Pino-Rios, *RSC Adv.*, 2022, **12**, 7906–7910.
42 R. Pino-Rios, A. Vásquez-Espinal, O. Yañez and W. Tiznado, *RSC Adv.*, 2020, **10**, 29705–29711.
43 M. Antić, B. Furtula and S. Radenković, *J. Phys. Chem. A*, 2017, **121**, 3616–3626.
44 M. Jirásek, M. Rickhaus, L. Tejerina and H. L. Anderson, *J. Am. Chem. Soc.*, 2021, **143**, 2403–2412.
45 L. Van Nyvel, M. Alonso and M. Solà, *Chem. Sci.*, 2025, **16**, 5613–5622.
46 A. D. Becke, *J. Chem. Phys.*, 1993, **98**, 5648–5652.
47 C. Lee, W. Yang and R. G. Parr, *Phys. Rev. B*, 1988, **37**, 785–789.
48 S. H. Vosko, L. Wilk and M. Nusair, *Can. J. Phys.*, 1980, **58**, 1200–1211.
49 F. Weigend and R. Ahlrichs, *Phys. Chem. Chem. Phys.*, 2005, **7**, 3297–3305.
50 M. J. Frisch, G. W. Trucks, H. B. Schlegel, G. E. Scuseria, M. A. Robb, J. R. Cheeseman, G. Scalmani, V. Barone, B. Mennucci, G. A. Petersson, H. Nakatsuji, M. Caricato, X. Li, H. P. Hratchian, A. F. Izmaylov, J. Bloino, G. Zheng, J. L. Sonnenberg, M. Hada, M. Ehara, K. Toyota, R. Fukuda, J. Hasegawa, M. Ishida, T. Nakajima, Y. Honda, O. Kitao, H. Nakai, T. Vreven, J. A. Montgomery, J. E. Peralta, F. Ogliaro, M. Bearpark, J. J. Heyd, E. Brothers, K. N. Kudin, V. N. Staroverov, R. Kobayashi, J. Normand, K. Raghavachari, A. Rendell, J. C. Burant, S. S. Iyengar, J. Tomasi, M. Cossi, N. Rega, J. M. Millam, M. Klene, J. E. Knox, J. B. Cross, V. Bakken, C. Adamo, J. Jaramillo, R. Gomperts, R. E. Stratmann, O. Yazyev, A. J. Austin, R. Cammi, C. Pomelli, J. W. Ochterski, R. L. Martin, K. Morokuma, V. G. Zakrzewski, G. A. Voth, P. Salvador, J. J. Dannenberg, S. Dapprich, A. D. Daniels, O. Farkas, J. B. Foresman, J. V. Ortiz, J. Cioslowski and D. J. Fox, *Gaussian 09, Revision B.01*, Gaussian Inc., Wallingford CT, 2009.
51 T. A. Keith and R. F. W. Bader, *Chem. Phys. Lett.*, 1993, **210**, 223–231.
52 T. A. Keith and R. F. W. Bader, *J. Chem. Phys.*, 1993, **99**, 3669–3682.
53 P. Lazzeretti, M. Malagoli and R. Zanasi, *Chem. Phys. Lett.*, 1994, **220**, 299–304.
54 E. Steiner and P. W. Fowler, *J. Phys. Chem. A*, 2001, **105**, 9553–9562.
55 U. Ayachit, *The ParaView Guide: A Parallel Visualization Application*, Kitware, 2015.
56 J. Jusélius, D. Sundholm and J. Gauss, *J. Chem. Phys.*, 2004, **121**, 3952–3963.
57 J. Cioslowski, E. Matito and M. Solà, *J. Phys. Chem. A*, 2007, **111**, 6521–6525.
58 T. Yanai, D. P. Tew and N. C. Handy, *Chem. Phys. Lett.*, 2004, **393**, 51–57.
59 A. D. Becke, *Phys. Rev. A*, 1988, **38**, 3098–3100.
60 J. P. Perdew, *Phys. Rev. B:Condens. Matter Mater. Phys.*, 1986, **33**, 8822–8824.
61 J.-D. Chai and M. Head-Gordon, *Phys. Chem. Chem. Phys.*, 2008, **10**, 6615–6620.
62 D. W. Szczepanik, *RunEDDB (version 11-Feb-2024)*, **http://aromaticity.eu**, accessed March 15, 2025.